



Article

# Protonic Transport in Layered Perovskites $\text{BaLa}_n\text{In}_n\text{O}_{3n+1}$ ( $n = 1, 2$ ) with Ruddlesden-Popper Structure

Nataliia Tarasova <sup>1,2,\*</sup> , Anzhelika Galisheva <sup>1,2</sup>, Irina Animitsa <sup>2</sup> , Daniil Korona <sup>2</sup>, Hala Kreimesh <sup>2</sup> and Irina Fedorova <sup>2</sup>

<sup>1</sup> The Institute of High Temperature Electrochemistry of the Ural Branch of the Russian Academy of Sciences, 620066 Ekaterinburg, Russia; a.o.galisheva@urfu.ru

<sup>2</sup> Institute of Natural Sciences and Mathematics, Ural Federal University, 620000 Yekaterinburg, Russia; irina.animitsa@urfu.ru (I.A.); d.v.korona@urfu.ru (D.K.); hala.loly.95@gmail.com (H.K.); irina-fedo\_19991999@mail.ru (I.F.)

\* Correspondence: natalia.tarasova@urfu.ru

**Abstract:** The work focused on the layered perovskite-related materials as the potential electrolytic components of such devices as proton conducting solid oxide fuel cells for the area of clean energy. The two-layered perovskite  $\text{BaLa}_2\text{In}_2\text{O}_7$  with the Ruddlesden–Popper structure was investigated as a protonic conductor for the first time. The role of increasing the amount of perovskite blocks in the layered structure on the ionic transport was investigated. It was shown that layered perovskites  $\text{BaLa}_n\text{In}_n\text{O}_{3n+1}$  ( $n = 1, 2$ ) demonstrate nearly pure protonic conductivity below 350 °C.

**Keywords:**  $\text{BaLaInO}_4$ ;  $\text{BaLa}_2\text{In}_2\text{O}_7$ ; layered perovskite; Ruddlesden-Popper structure; water uptake; oxygen-ion conductivity; protonic conductivity; the proton conducting solid oxide fuel cells



**Citation:** Tarasova, N.; Galisheva, A.; Animitsa, I.; Korona, D.; Kreimesh, H.; Fedorova, I. Protonic Transport in Layered Perovskites  $\text{BaLa}_n\text{In}_n\text{O}_{3n+1}$  ( $n = 1, 2$ ) with Ruddlesden-Popper Structure. *Appl. Sci.* **2022**, *12*, 4082. <https://doi.org/10.3390/app12084082>

Academic Editor: Guntae Kim

Received: 17 January 2022

Accepted: 14 April 2022

Published: 18 April 2022

**Publisher's Note:** MDPI stays neutral with regard to jurisdictional claims in published maps and institutional affiliations.



**Copyright:** © 2022 by the authors. Licensee MDPI, Basel, Switzerland. This article is an open access article distributed under the terms and conditions of the Creative Commons Attribution (CC BY) license (<https://creativecommons.org/licenses/by/4.0/>).

## 1. Introduction

The rising of the environmental challenges and the increasing in the need for safe and effective devices for energy conversion and storage mark the new decade [1–4]. This makes the task of creating high-efficiency solid oxide devices for electrochemical applications very important for now. The oxygen- and proton-conducting solid oxides may be components of various devices including fuel cells and electrolyzers [5–21]. Most well-known electrolytes for medium-temperature solid oxide fuel cells (500–700 °C) are characterized by the perovskite or perovskite-related structure  $\text{ABO}_{3-\delta}$  [22]. As an example, one of the most investigated protonic conductors, barium zirconate [23], has the structure of ordinary perovskite with a cubic unit cell (Figure 1a). The varying of the cations A and B can create the materials with a layered perovskite-related structure where the perovskite layers alternate with rock-salt layers.

The general formula of layered perovskite-related structures can be written as  $\text{AO}(\text{A}'\text{BO}_3)_n$ , where  $n$  is the number of polyhedra layers stacking in the perovskite block. When  $n = 1$ , this formula can be represented as  $\text{AA}'\text{BO}_4$ , and the compositions with this formula are characterized by the monolayered perovskite-related structure. The family of proton-conducting oxides with this type of the structure was discovered several years ago, and it is represented by the matrix compositions  $\text{SrLaInO}_4$  [24–28],  $\text{BaLaInO}_4$  [29–37],  $\text{BaNdInO}_4$  [38–43],  $\text{BaNdScO}_4$  [44]. The symmetry of these compositions is lower than cubic, and it is orthorhombic or monoclinic depending on the combination of cations in the A and B sublattices. As an example, the orthorhombic structure of the compound  $\text{BaLaInO}_4$  is represented in Figure 1b. It was shown that various types of doping (donor and acceptor) lead to the increase in the values of ionic conductivity [45]. Moreover, the compositions based on  $\text{BaLaInO}_4$  demonstrate almost pure protonic conductivity under wet air conditions at 450 °C [45].

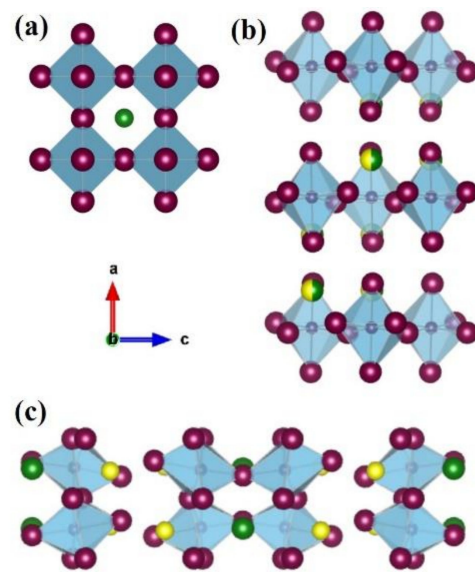


**Figure 1.** Structure of  $\text{BaZrO}_3$  ( $\text{ABO}_3$ ) (a),  $\text{BaLaInO}_4$  ( $\text{AA}'\text{BO}_4$ ) (b) and  $\text{BaLa}_2\text{In}_2\text{O}_7$  ( $\text{AA}'_2\text{B}_2\text{O}_7$ ) (c), where red spheres represent the oxygen atoms; green spheres represent the atoms of A-sublattice; and yellow spheres represent the atoms of A'-sublattice.

The next member of the homologous series of the Ruddlesden–Popper type of structure with  $n = 2$  can be written in the general case as  $\text{AA}'_2\text{B}_2\text{O}_7$  and as an example  $\text{BaLa}_2\text{In}_2\text{O}_7$ . Despite the possibility of protonic transport in the two-layered complex oxide,  $\text{BaLa}_2\text{In}_2\text{O}_7$  is not yet described; the structure of  $\text{BaLa}_n\text{In}_n\text{O}_{3n+1}$  ( $n = 1, 2$ ) is described in detail by Titov et al. [46] and Raveau et al. [47]. One of the main differences between  $\text{BaLaInO}_4$  and  $\text{BaLa}_2\text{In}_2\text{O}_7$  compositions is the ratio of perovskite blocks and rock-salt layers in the unit cell. This ratio is 1:1 for  $\text{BaLaInO}_4$  and 2:1 for  $\text{BaLa}_2\text{In}_2\text{O}_7$ . It can be assumed that an increase in the ratio of perovskite blocks can lead to the increase in the ionic conductivity of solid oxide. Based on this, the goal of this work is the investigation of ionic transport ( $\text{O}^{2-}$ ,  $\text{H}^+$ ) in the two-layered compound  $\text{BaLa}_2\text{In}_2\text{O}_7$  in comparison with the mono-layered compound  $\text{BaLaInO}_4$ . Proton transport is not previously reported for  $n = 2$  RP phases in the Ba-La-In-O system.

## 2. Experimental

The phase  $\text{BaLa}_2\text{In}_2\text{O}_7$  was synthesized using the solid state method. The previously dried powder reagents  $\text{BaCO}_3$ ,  $\text{La}_2\text{O}_3$ ,  $\text{In}_2\text{O}_3$  were used as starting materials. The milling of the reagents was made in an agate mortar. The calcination was performed in the temperature range from 800 to 1300 °C with the step of 100 °C and 24 h time treatments.

The XRD studies were performed using a Bruker Advance D8 (Rheinstetten, Germany) diffractometer with  $\text{Cu K}\alpha$  radiation over a range from 20° to 100° with a step of 0.01° and at a scanning rate of 0.5°/min. The preparation of the samples was made by their heating at 1100 °C for 5 h and following cooling in dry Ar ( $p_{\text{H}_2\text{O}} = 3.5 \times 10^{-5}$  atm).

For the investigations of the electrical properties, the pressed cylindrical pellets (1300 °C, 24 h, dry air) were obtained. The pellets had a relative density ~92% (density of the sintered samples was determined by the Archimedes' method). The  $ac$  conductivity measurements were performed by the Z-1000P (Elins, Russian Federation) impedance spectrometer within the frequency range of 1–10<sup>6</sup> Hz. Electrical measurements were performed using Pt paste electrodes (annealing at 1000 °C for 2 h). The temperature dependencies of conductivities were obtained in the temperature range 200–1000 °C (step 10–20 °C, cooling rate of 1°/min; the measurements were taken until a constant resistance value was established). These investigations were performed under “dry” and “wet” air or Ar. The dry gas was produced by circulating the gas through  $\text{P}_2\text{O}_5$  ( $p_{\text{H}_2\text{O}} = 3.5 \times 10^{-5}$  atm). The wet gas was obtained by bubbling the gas at room temperature first through distilled

water and then through a saturated solution of KBr ( $p_{\text{H}_2\text{O}} = 2 \times 10^{-2}$  atm). The humidity of the gas was controlled by a Honeywell HIH-3610  $\text{H}_2\text{O}$ -sensor. The dependencies of conductivities vs. partial oxygen pressures  $p_{\text{O}_2}$  were obtained by using the electrochemical method for producing different  $p_{\text{O}_2}$  with an oxygen pump (and sensor) from Y-stabilized  $\text{ZrO}_2$  ceramic. Each resistance value was recorded after 3–5 h of equilibrium.

### 3. Results and Discussions

The phase characterization of the obtained sample  $\text{BaLa}_2\text{In}_2\text{O}_7$  was made using XRD analysis. It was shown that all observed diffraction peaks can be related to the single phase belonging to the tetragonal symmetry (space group  $P4_2/mnm$ ) (Figure 2). The lattice parameters ( $a = 5.914(9)$  Å,  $c = 20.846(5)$  Å) were in good agreement with those previously reported by Titov et al. and Raveau et al. ( $a = 5.915(2)$  Å,  $c = 20.86(1)$  Å [46];  $a = 5.9141(3)$  Å,  $c = 20.8231(2)$  [47]). The structural parameters are presented in the Table 1.

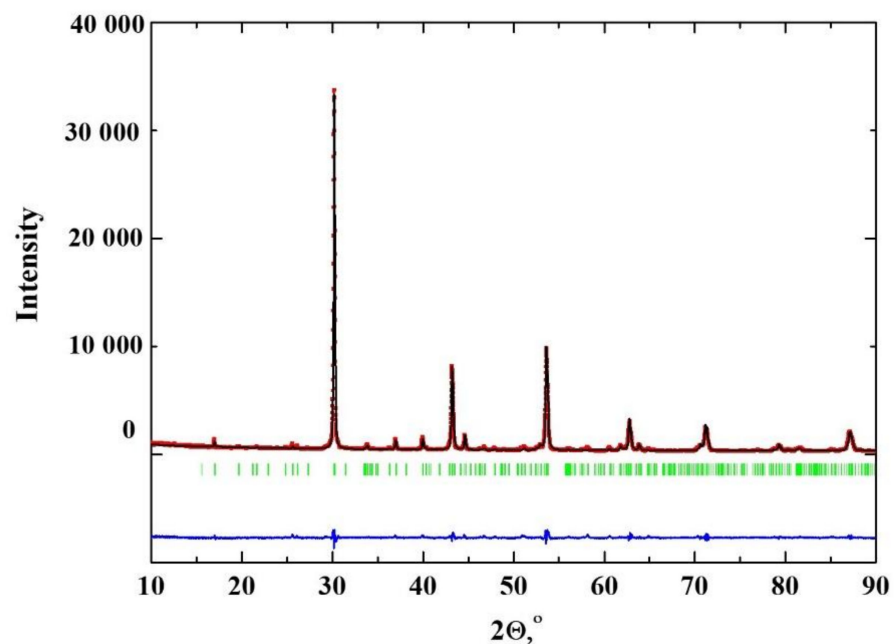


Figure 2. The XRD-data for the composition  $\text{BaLa}_2\text{In}_2\text{O}_7$ .

Table 1. Refined structural parameters from XRD-data.

Atom	Site	x	y	z
Ba	4f	0.2483(1)	0.2483(1)	0
La	8j	0.2687(4)	0.2687(4)	0.1851(3)
In	8j	0.2590(0)	0.2590(0)	0.4002(2)
O(1)	4g	0.806(1)	0.193(3)	0
O(2)	8j	0.183(4)	0.183(4)	0.291(1)
O(3)	8h	0	0.5	0.095(2)
O(4)	4e	0	0	0.126(1)
O(5)	4e	0	0	0.382(1)

$$R_p = 4.31, R_{wp} = 3.48, \chi^2 = 1.73.$$

The 3D visualization of the crystal structure of the obtained phase is presented in the Figure 1c using VESTA software [48]. As can be seen (Figure 1), for the mono-layered structure (Figure 1b), the ordering in the A and A' cations does not happen, and Ba and La atoms occupy the same positions in the crystal lattice of  $\text{BaLaInO}_4$ , and they have the same coordination number (c.n. = 9). Opposite, the ordered arrangement of A and A' cations is observed for the two-layered complex oxide  $\text{BaLa}_2\text{In}_2\text{O}_7$ , as it was shown by Raveau et al. [47] with using high resolution electron microscopy (Figure 1c). It was

confirmed that barium atoms locate in the perovskite blocks, and the lanthanum atoms are placed in the rock-salt layers [47]. In the case of the two-layered structure, the cation with the largest ionic radii (barium in this case) has the c.n. = 12 and forms polyhedra  $[\text{BaO}_{12}]$ ; the cation with lower ionic radii (lanthanum) forms the polyhedra  $(\text{LaO}_9)$  with c.n. = 9. However, it was shown that both perovskite blocks and rock-salt layers are distorted, and the real coordination numbers are ten and seven for barium and lanthanum, respectively [47].

The electrical conductivity was measured by the impedance spectroscopy method. The Nyquist-plots for the investigated composition  $\text{BaLa}_2\text{In}_2\text{O}_7$  obtained under dry air are presented in Figure 3a–c. The fitting of the spectra was made using ZView software, and the obtained results are presented in Table 2. According to the fitting of the spectra (red line) with using the equivalent circuit presented in Figure 3d, three different electrochemical processes can be defined. For the calculation of electrical conductivity, the bulk resistance values  $R_1$  were used and are discussed below. It can be noted that, due to the small depression of the semicircles, the constant phase element (CPE) was used during the analysis of Nyquist plots.

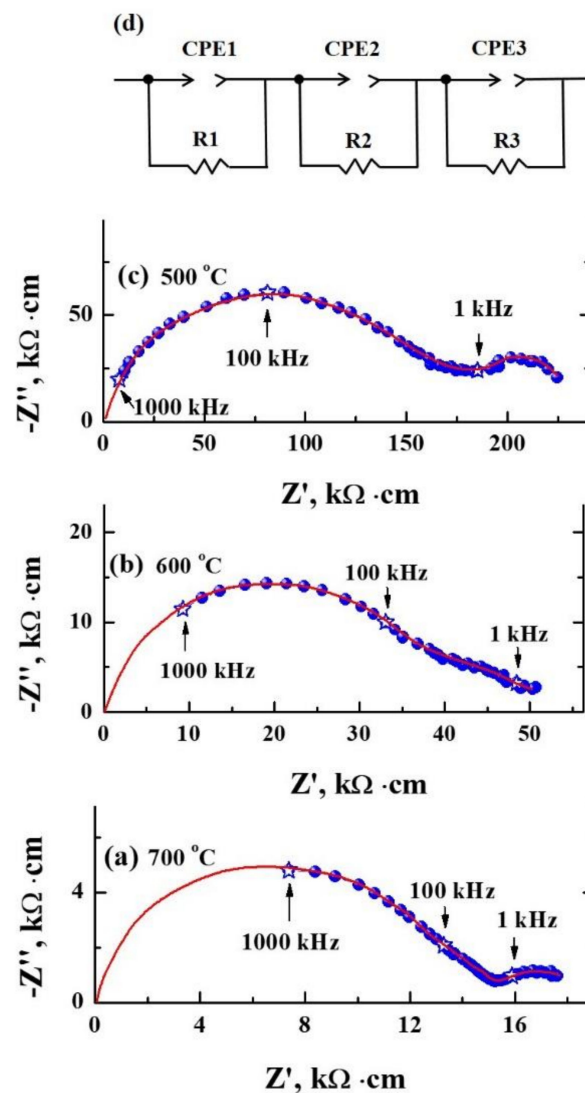


**Figure 3.** The Nyquist-plots obtained at the different temperatures under dry air for the composition  $\text{BaLa}_2\text{In}_2\text{O}_7$ : (a) 700 °C, (b) 600 °C, (c) 500 °C, and (d) the equivalent circuit of fitting (red line).

**Table 2.** Results of Nyquist-plots fitting, where CPE is the constant phase element (F), and R is the resistance (kΩ·cm).

Element	Value (700 °C)	Value (600 °C)	Value (500 °C)
CPE1	$2.1 \times 10^{-12}$	$2.4 \times 10^{-12}$	$3.2 \times 10^{-12}$
R1	13	36	158
CPE2	$4.1 \times 10^{-10}$	$3.7 \times 10^{-10}$	$2.1 \times 10^{-10}$
R2	2	8	33
CPE3	$6.0 \times 10^{-7}$	$5.6 \times 10^{-7}$	$7.0 \times 10^{-7}$
R3	3	7	39

The temperature dependencies of bulk conductivities obtained under dry air and dry Ar are presented in Figure 4. As can be seen, the conductivity values for the compound BaLa<sub>2</sub>In<sub>2</sub>O<sub>7</sub> are higher than for BaLaInO<sub>4</sub> [29] by around 0.6–0.7 order of magnitude. This confirms the previously stated assumption that the increase in the ratio of perovskite blocks in the layered structures can lead to the increase in the electrical conductivity values. However, for the correct comparison, the total conductivity values must be divided into ionic and electronic contributions.

To establish the nature of electrical transport in BaLa<sub>2</sub>In<sub>2</sub>O<sub>7</sub>, the conductivity measurements vs.  $pO_2$  were performed (Figure 5). As can be seen (Figure 5a), in the electrolytic area ( $pO_2 = 10^{-16}$ – $10^{-5}$  atm), the independence of conductivity values from  $pO_2$  was observed. Thus, the oxygen-ionic conductivity dominates in this region. For layered structures, oxygen-ionic transport is usually described in terms of anti-Frenkel disordering:



where  $O_i''$  is the oxygen atom in the interstitial position;  $V_O^{\bullet\bullet}$  is the oxygen vacancy.

The possibility of the formation of interstitial oxygen is provided by the existence of a rock-salt block and the possibility of increasing the coordination number of the cation that is located there. Accordingly, the formation of oxygen vacancies occurs in the perovskite block; the cation, octahedrally surrounded by oxygen, lowers the coordination number. That is, the presence of oxygen-deficient perovskite blocks plays an important role in the formation of oxygen-ion transport. Therefore, for such structures, it is possible to expect a significant oxygen-ionic conductivity without doping. Moreover, the measurements of the conductivity versus  $pO_2$  showed that the phases of BaLa<sub>2</sub>In<sub>2</sub>O<sub>7</sub> are stable over a wide range of  $pO_2$ .

The conductivity dependencies obtained in the dry oxidizing conditions ( $pO_2 = 10^{-5}$ –0.21 atm) have a positive slope, which indicates the mixed ionic–electronic (hole) nature of conductivity:



where  $O_i''$  is the oxygen atom in the interstitial position;  $V_O^{\bullet\bullet}$  is the oxygen vacancy;  $h^\bullet$  is the hole. Obviously, both of these processes can be realized in the structure. However, it is impossible to say which process prevails. For the layered composition based on BaNdInO<sub>4</sub>, the calculations of formation energies of point defects were made [41]. The energy of processes described by Equation (3) is about 1.2 eV. However, the data for Equation (2) are missing.

It should be noted that the conductivity values obtained in the dry Ar (blue symbols in the Figure 5) are the same as the conductivity values from the electrolytic area (black symbols in the Figure 5a). Therefore, in an argon atmosphere, it is relatively easy to measure the temperature dependence of oxygen-ionic conductivity in a wide temperature range.

It was shown earlier, for the compositions based on BaLaInO<sub>4</sub>, the conductivity values obtained under dry Ar corresponded to the oxygen-ionic conductivity values [45]. Based on this, the oxygen-ionic transport number  $t_{O^{2-}}$  can be calculated as:

$$t_{O^{2-}} = \frac{\sigma_{O^{2-}}}{\sigma_{tot}} = \frac{\sigma_{Ar}}{\sigma_{air}} \tag{4}$$

The oxygen-ionic transport numbers for both BaLa<sub>2</sub>In<sub>2</sub>O<sub>7</sub> and BaLaInO<sub>4</sub> compositions did not change under temperature variation at  $p_{O_2} = 0.21$  atm and were around 20% for each composition, and both compositions demonstrate mixed ionic-electronic (hole) conductivity under dry air, as it was shown earlier for the composition BaLaInO<sub>4</sub> [45].

Returning to Figure 4a, it can be seen that the values of oxygen-ionic conductivity for BaLa<sub>2</sub>In<sub>2</sub>O<sub>7</sub> were higher than for BaLaInO<sub>4</sub>. It should be noted that the increasing in the oxygen-ionic conductivity values correlates well with the decreasing in the values of energy activation of oxygen transport (from 0.87 eV for BaLaInO<sub>4</sub> to 0.81 eV for BaLaInO<sub>4</sub>). Because the increase in the oxygen-ionic conductivity correlates with the increase in the number of perovskite layers in the structure, we can suppose that the transport of oxygen ions includes the oxygen positions in the In-containing polyhedra.

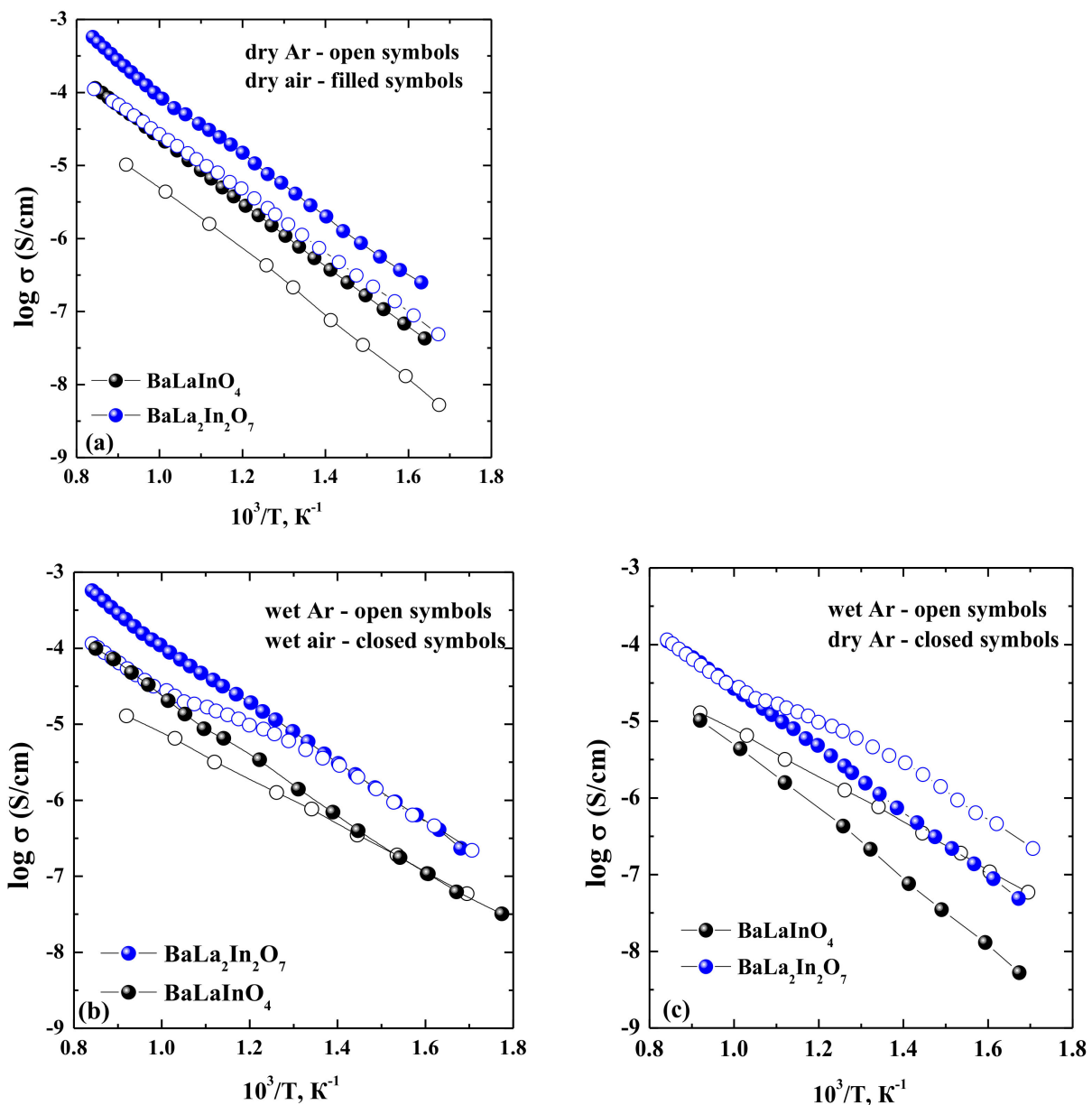


**Figure 4.** The temperature dependencies of conductivity of BaLa<sub>2</sub>In<sub>2</sub>O<sub>7</sub> (blue symbols) and BaLaInO<sub>4</sub> (black symbols) [29] obtained dry Ar (open symbols) and dry air (closed symbols) (a), wet Ar (open symbols) and wet air (closed symbols) (b), wet Ar (open symbols), and dry Ar (closed symbols) (c).



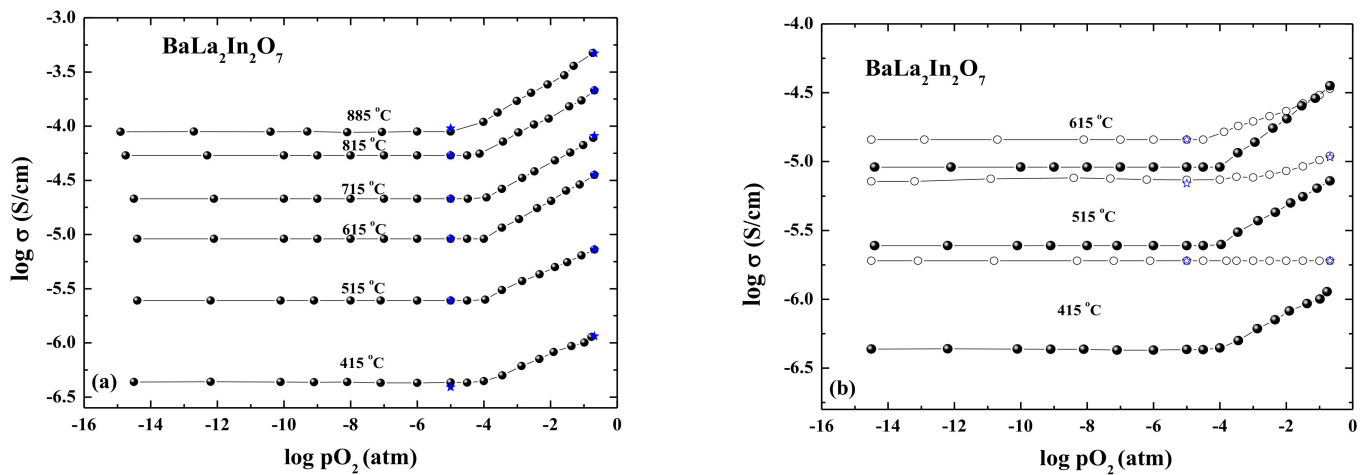
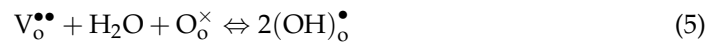


**Figure 5.** The dependencies of the conductivity values vs.  $pO_2$  for the sample  $BaLa_2In_2O_7$  at dry conditions (a) and dry (closed symbols) and wet (open symbols) conditions (b) (black symbols) and conductivity values from  $\sigma-10^3/T$  dependencies at dry Ar (blue symbols).

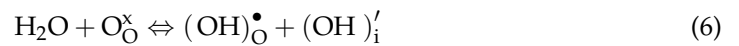
The comparison of the dependencies of conductivity vs. oxygen partial pressure under dry and wet conditions is presented in Figure 5b. At the  $pO_2$  range from  $10^{-4}$  to  $10^{-16}$  atm, the conductivity increases significantly in a wet atmosphere as a result of the appearance of a proton contribution due to the dissolution of  $H_2O$  in  $BaLa_2In_2O_7$ .

Water molecules can be dissolved in the oxygen-deficient perovskite layers leading to the formation of proton carriers as follows:



where  $V_o^{\bullet\bullet}$  is the oxygen vacancy;  $O_o^\times$  is the oxygen atom in the regular position;  $(OH)_o^\bullet$  is the hydroxyl group in the oxygen sublattice.

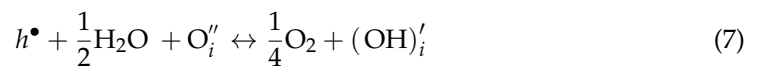
At the same time, for layered structures containing rock-salt blocks, the second mechanism of the dissociative dissolution of water molecules is possible:



where  $(OH)_o^\bullet$  is the hydroxyl group in the regular oxygen position;  $(OH)_i'$  is the hydroxyl group located in the rock-salt block. This process is accompanied by the increase in the coordination number of atoms in the rock-salt block.

The increase in the conductivity in a wet atmosphere compared to a dry atmosphere is reduced with increasing temperature. In a wet atmosphere below 450 °C, the conductivity does not depend on  $pO_2$ , which reflects the dominant ionic (proton) nature of the conductivity.

Differences in the conductivities in dry and wet atmospheres at high  $pO_2 > 10^{-4}$  atm are not so significant compared to the plateau region (Figure 5b). This is due to the presence of holes, the concentration of which decreases in a wet atmosphere:



where  $h^\bullet$  is the hole;  $O_i''$  is the oxygen atom in the interstitial position;  $(OH)_i'$  is the oxygen-hydrogen group.

In accordance with the explanations presented above and the obtained data on conductivity- $pO_2$ , the measurements of conductivity in a wide temperature range can be carried out by comparing the atmosphere of air and argon at different levels of humidity. This comparison is shown in Figure 4.

As can be seen (Figure 4b), the values of ionic conductivity (wet Ar) are near the same as the total conductivity values (wet air) below ~450 °C. In other words, the nature of conductivity changes from mixed ionic-hole (dry air) to predominantly ionic (wet air,  $T < 450$  °C).

The difference between conductivity values obtained under atmospheres with different water partial pressures is well visible for the Ar atmosphere, and these temperature dependencies are presented in Figure 4c. The protonic transport numbers  $t_p$  were calculated according to the equation:

$$t_p = \frac{\sigma_{wet\ Ar} - \sigma_{dry\ Ar}}{\sigma_{wet}} \quad (8)$$

which was used earlier by Y. Zhou et al. [43] for the layered perovskites based on BaNdInO<sub>4</sub>. It was established that for both compositions BaLa<sub>2</sub>In<sub>2</sub>O<sub>7</sub> and BaLaInO<sub>4</sub>, the protonic transport numbers increase with a decreasing temperature and reach ~90–95% in the temperature range 300–350 °C.

Therefore, the possibility of protonic transport in the two-layered complex oxide BaLa<sub>2</sub>In<sub>2</sub>O<sub>7</sub> with the Ruddlesden–Popper structure was shown for the first time. It was proved that an increase in  $n$  in the formula BaLa <sub>$n$</sub> In <sub>$n$</sub> O<sub>3 $n$ +1</sub> leads to the increase in the ionic conductivity. The composition BaLa<sub>2</sub>In<sub>2</sub>O<sub>7</sub> demonstrates nearly pure protonic conductivity under wet air below 350 °C. This allows for considering this complex oxide as a promising matrix composition for obtaining novel high-conductive protonic electrolytes based on it.

#### 4. Conclusions

In this work, the complex oxide BaLa<sub>2</sub>In<sub>2</sub>O<sub>7</sub> was synthesized, and the electrical conductivity was measured for the first time. It was shown that change in the ratio between perovskite blocks and rock-salt layers in the layered perovskite-related complex oxides BaLa <sub>$n$</sub> In <sub>$n$</sub> O<sub>3 $n$ +1</sub> ( $n = 1, 2$ ) influences the ionic conductivity values. The increasing  $n$  in the formula leads to the increase in the ionic conductivity due to the increase in the share of perovskite blocks. It was proved that the complex oxide BaLa<sub>2</sub>In<sub>2</sub>O<sub>7</sub> demonstrates nearly pure protonic conductivity under wet air below 350 °C, and it can be considered as the promising compound for obtaining novel high-conductive protonic electrolytes based on it.

**Author Contributions:** Conceptualization, I.A. and N.T.; methodology, I.A. and N.T.; investigation, A.G., D.K., H.K. and I.F.; data curation, N.T. and A.G.; writing—original draft preparation, N.T.; writing—review and editing, N.T. and I.A. All authors have read and agreed to the published version of the manuscript.

**Funding:** This research received no external funding.

**Institutional Review Board Statement:** Not applicable.

**Informed Consent Statement:** Not applicable.

**Data Availability Statement:** Not applicable.

**Conflicts of Interest:** The authors declare no conflict of interest.

#### References

1. Corvalan, C.; Prats, E.V.; Sena, A.; Varangu, L.; Vinci, S. Towards Climate Resilient and Environmentally Sustainable Health Care Facilities. *Int. J. Environ. Res. Public Health* **2020**, *17*, 8849. [CrossRef]
2. Watts, N.; Amann, M.; Arnell, N.; Montgomery, H.; Costello, A. The 2020 report of The Lancet Countdown on health and climate change: Responding to converging crises. *Lancet* **2021**, *397*, 129–170. [CrossRef]
3. Afroze, S.; Reza, M.S.; Cheok, Q.; Taweekun, J.; Azad, A.K. Solid oxide fuel cell (SOFC); A new approach of energy generation during the pandemic COVID-19. *Int. J. Integr. Eng.* **2020**, *12*, 245–256. [CrossRef]
4. Afroze, S.; Reza, M.S.; Cheok, Q.; Islam, S.N.; Abdalla, A.M.; Taweekun, J.; Azad, A.K.; Khalilpoor, N.; Issakhov, A. Advanced Applications of Fuel Cells during the COVID-19 Pandemic. *Int. J. Chem. Eng.* **2021**, *2021*, 5539048. [CrossRef]
5. Sun, C.; Alonso, J.A.; Bian, J. Recent Advances in Perovskite-Type Oxides for Energy Conversion and Storage Applications. *Adv. Energy Mater.* **2020**, *11*, 2000459. [CrossRef]
6. Shi, H.; Su, C.; Ran, R.; Cao, J.; Shao, Z. Electrolyte materials for intermediate-temperature solid oxide fuel cells. *Prog. Nat. Sci. Mater. Int.* **2020**, *30*, 764–774. [CrossRef]
7. Yang, B.; Guo, Z.; Wang, J.; Wang, J.; Zhu, T.; Shu, H.; Qiu, G.; Chen, J.; Zhang, J. Solid oxide fuel cell systems fault diagnosis: Critical summarization, classification, and perspectives. *J. Energy Storage* **2021**, *34*, 102153. [CrossRef]
8. Peng, J.; Huang, J.; Wu, X.-L.; Xu, Y.-W.; Chen, H.; Li, X. Solid oxide fuel cell (SOFC) performance evaluation, fault diagnosis and health control: A review. *J. Power Sources* **2021**, *5051*, 230058. [CrossRef]



9. Ding, P.; Li, W.; Zhao, H.; Wu, C.; Zhao, L.; Dong, B.; Wang, S. Review on Ruddlesden-Popper perovskites as cathode for solid oxide fuel cells. *J. Phys. Mater.* **2021**, *4*, 022002. [[CrossRef](#)]
10. Singh, M.; Zappa, D.; Comini, E. Solid oxide fuel cell: Decade of progress, future perspectives and challenges. *Int. J. Hydrogen Energy* **2021**, *46*, 27643–276745. [[CrossRef](#)]
11. Shen, M.; Ai, F.; Ma, H.; Xu, H.; Zhang, Y. Progress and prospects of reversible solid oxide fuel cell materials. *iScience* **2021**, *24*, 103464. [[CrossRef](#)]
12. Kim, S.; Kim, G.; Manthiram, A. A review on infiltration techniques for energy conversion and storage devices: From fundamentals to applications. *Sustain. Energy Fuels* **2021**, *5*, 5024–5037. [[CrossRef](#)]
13. Klyndyuk, A.I.; Chizhova, E.A.; Kharytonau, D.S.; Medvedev, D.A. Layered oxygen-deficient double perovskites as promising cathode materials for solid oxide fuel cells. *Materials* **2022**, *15*, 141. [[CrossRef](#)]
14. Hanif, M.B.; Motola, M.; Qayyum, S.; Rauf, S.; Khalid, A.; Li, C.-J.; Li, C.-X. Recent advancements, doping strategies and the future perspective of perovskite-based solid oxide fuel cells for energy conversion. *Chem. Eng. J.* **2022**, *42815*, 132603. [[CrossRef](#)]
15. Medvedev, D. Trends in research and development of protonic ceramic electrolysis cells. *Int. J. Hydrogen Energy* **2019**, *44*, 26711–26740. [[CrossRef](#)]
16. Shim, J.H. Ceramics breakthrough. *Nat. Energy* **2018**, *3*, 168–169. [[CrossRef](#)]
17. Meng, Y.; Gao, J.; Zhao, Z.; Amoroso, J.; Tong, J.; Brinkman, K.S. Review: Recent progress in low-temperature proton-conducting ceramics. *J. Mater. Sci.* **2019**, *54*, 9291–9312. [[CrossRef](#)]
18. Kim, J.; Sengodan, S.; Kim, S.; Kwon, O.; Bud, Y.; Kim, G. Proton conducting oxides: A review of materials and applications for renewable energy conversion and storage. *Renew. Sustain. Energy Rev.* **2019**, *109*, 606–618. [[CrossRef](#)]
19. Zvonareva, I.; Fu, X.-Z.; Medvedev, D.; Shao, Z. Electrochemistry and energy conversion features of protonic ceramic cells with mixed ionic-electronic electrolytes. *Energy Environ. Sci.* **2022**, *15*, 439–465. [[CrossRef](#)]
20. Medvedev, D.A. Current drawbacks of proton-conducting ceramic materials: How to overcome them for real electrochemical purposes. *Curr. Opin. Green Sustain. Chem.* **2021**, *32*, 100549. [[CrossRef](#)]
21. Bello, I.T.; Zhai, S.; He, Q.; Cheng, C.; Dai, Y.; Chen, B.; Zhang, Y.; Ni, M. Materials development and prospective for protonic ceramic fuel cells. *Int. J. Energy Res.* **2021**, *46*, 2212–2240. [[CrossRef](#)]
22. Irvine, J.; Rupp, J.L.; Liu, G.; Xu, X.; Haile, S.; Qian, X.; Snyder, A.; Freer, R.; Ekren, D.; Skinner, S. Roadmap on inorganic perovskites for energy applications. *J. Phys. Energy* **2021**, *3*, 031502. [[CrossRef](#)]
23. Hossain, M.K.; Chanda, R.; El-Denglawey, A.; Emrose, T.; Rahman, M.T.; Biswas, M.C.; Hashizume, K. Recent progress in barium zirconate proton conductors for electrochemical hydrogen device applications: A review. *Ceram. Int.* **2021**, *47*, 23725–23748. [[CrossRef](#)]
24. Kato, S.; Ogasawara, M.; Sugai, M.; Nakata, S. Synthesis and oxide ion conductivity of new layered perovskite  $\text{La}_{1-x}\text{Sr}_{1+x}\text{InO}_{4-d}$ . *Solid State Ion.* **2002**, *149*, 53–57. [[CrossRef](#)]
25. Troncoso, L.; Alonso, J.A.; Aguadero, A. Low activation energies for interstitial oxygen conduction in the layered perovskites  $\text{La}_{1+x}\text{Sr}_{1-x}\text{InO}_{4+d}$ . *J. Mater. Chem. A* **2015**, *3*, 17797–17803. [[CrossRef](#)]
26. Troncoso, L.; Alonso, J.A.; Fernández-Díaz, M.T.; Aguadero, A. Introduction of interstitial oxygen atoms in the layered perovskite  $\text{LaSrIn}_{1-x}\text{BxO}_{4+\delta}$  system (B=Zr, Ti). *Solid State Ion.* **2015**, *282*, 82–87. [[CrossRef](#)]
27. Troncoso, L.; Mariño, C.; Arce, M.D.; Alonso, J.A. Dual Oxygen Defects in Layered  $\text{La}_{1.2}\text{Sr}_{0.8-x}\text{BaxInO}_{4+d}$  ( $x = 0.2, 0.3$ ) Oxide-Ion Conductors: A Neutron Diffraction Study. *Materials* **2019**, *12*, 1624. [[CrossRef](#)] [[PubMed](#)]
28. Troncoso, L.; Arce, M.D.; Fernández-Díaz, M.T.; Moggi, L.V.; Alonso, J.A. Water insertion and combined interstitial-vacancy oxygen conduction in the layered perovskites  $\text{La}_{1.2}\text{Sr}_{0.8-x}\text{BaxInO}_{4+\delta}$ . *New J. Chem.* **2019**, *43*, 6087–6094. [[CrossRef](#)]
29. Tarasova, N.; Animitsa, I.; Galisheva, A.; Korona, D. Incorporation and Conduction of Protons in Ca, Sr, Ba-Doped  $\text{BaLaInO}_4$  with Ruddlesden-Popper Structure. *Materials* **2019**, *12*, 1668. [[CrossRef](#)]
30. Tarasova, N.; Animitsa, I.; Galisheva, A.; Pryakhina, V. Protonic transport in the new phases  $\text{BaLaIn}_{0.9}\text{M}_{0.1}\text{O}_{4.05}$  (M=Ti, Zr) with Ruddlesden-Popper structure. *Solid State Sci.* **2020**, *101*, 106121. [[CrossRef](#)]
31. Tarasova, N.; Animitsa, I.; Galisheva, A. Electrical properties of new protonic conductors  $\text{Ba}_{1+x}\text{La}_{1-x}\text{InO}_{4-0.5x}$  with Ruddlesden-Popper structure. *J. Solid State Electrochem.* **2020**, *24*, 1497–1508. [[CrossRef](#)]
32. Tarasova, N.; Galisheva, A.; Animitsa, I. Improvement of oxygen-ionic and protonic conductivity of  $\text{BaLaInO}_4$  through Ti doping. *Ionics* **2020**, *26*, 5075–5088. [[CrossRef](#)]
33. Tarasova, N.; Galisheva, A.; Animitsa, I.  $\text{Ba}^{2+}/\text{Ti}^{4+}$ -co-doped layered perovskite  $\text{BaLaInO}_4$ : The structure and ionic ( $\text{O}^{2-}$ ,  $\text{H}^+$ ) conductivity. *Int. J. Hydrogen Energy* **2021**, *46*, 16868–16877. [[CrossRef](#)]
34. Tarasova, N.A.; Galisheva, A.O.; Animitsa, I.E.; Lebedeva, E.L. Oxygen-Ion and Proton Transport in Sc-Doped Layered Perovskite  $\text{BaLaInO}_4$ . *Russ. J. Electrochem.* **2021**, *57*, 1008–1014. [[CrossRef](#)]
35. Tarasova, N.A.; Galisheva, A.O.; Animitsa, I.E.; Dmitrieva, A.A. The Effect of Donor Doping on the Ionic ( $\text{O}^{2-}$ ,  $\text{H}^+$ ) Transport in Novel Complex Oxides  $\text{BaLaIn}_{1-x}\text{Nb}_x\text{O}_{4+x}$  with the Ruddlesden-Popper Structure. *Russ. J. Electrochem.* **2021**, *57*, 962–969. [[CrossRef](#)]
36. Tarasova, N.; Animitsa, I.; Galisheva, A. Effect of acceptor and donor doping on the state of protons in block-layered structures based on  $\text{BaLaInO}_4$ . *Solid State Comm.* **2021**, *323*, 14093. [[CrossRef](#)]
37. Tarasova, N.; Animitsa, I.; Galisheva, A. Spectroscopic and transport properties of Ba- and Ti-doped  $\text{BaLaInO}_4$ . *J. Raman Spec.* **2021**, *52*, 980–987. [[CrossRef](#)]

38. Fujii, K.; Esaki, Y.; Omoto, K.; Yashima, M.; Hoshikawa, A.; Ishigaki, T.; Hester, J.R. New Perovskite-Related Structure Family of Oxide-Ion Conducting Materials NdBaInO<sub>4</sub>. *Chem. Mater.* **2014**, *26*, 2488–2491. [[CrossRef](#)]
39. Fujii, K.; Shiraiwa, M.; Esaki, Y.; Yashima, M.; Kim, S.J.; Lee, S. Improved oxide-ion conductivity of NdBaInO<sub>4</sub> by Sr doping. *J. Mater. Chem. A* **2015**, *3*, 11985. [[CrossRef](#)]
40. Ishihara, T.; Yan, Y.; Sakai, T.; Ida, S. Oxide ion conductivity in doped NdBaInO<sub>4</sub>. *Solid State Ion.* **2016**, *288*, 262–265. [[CrossRef](#)]
41. Yang, X.; Liu, S.; Lu, F.; Xu, J.; Kuang, X. Acceptor Doping and Oxygen Vacancy Migration in Layered Perovskite NdBaInO<sub>4</sub>-Based Mixed Conductors. *J. Phys. Chem. C* **2016**, *120*, 6416–6426. [[CrossRef](#)]
42. Fujii, K.; Yashima, M. Discovery and development of BaNdInO<sub>4</sub> -A brief review. *J. Ceram. Soc. Jpn.* **2018**, *126*, 852–859. [[CrossRef](#)]
43. Zhou, Y.; Shiraiwa, M.; Nagao, M.; Fujii, K.; Tanaka, I.; Yashima, M.; Baque, L.; Basbus, J.F.; Moggi, L.V.; Skinner, S.J. Protonic Conduction in the BaNdInO<sub>4</sub> Structure Achieved by Acceptor Doping. *Chem. Mater.* **2021**, *33*, 2139–2146. [[CrossRef](#)]
44. Shiraiwa, M.; Kido, T.; Fujii, K.; Yashima, M. High-temperature proton conductors based on the (110) layered perovskite BaNdScO<sub>4</sub>. *J. Mat. Chem. A* **2021**, *9*, 8607. [[CrossRef](#)]
45. Tarasova, N.; Animitsa, I. Materials A<sup>II</sup>LnInO<sub>4</sub> with Ruddlesden-Popper structure for electrochemical applications: Relationship between ion (oxygen-ion, proton) conductivity, water uptake and structural changes. *Materials* **2022**, *15*, 114. [[CrossRef](#)] [[PubMed](#)]
46. Titov, Y.A.; Belyavina, N.M.; Markiv, V.Y.; Slobodyanik, M.S.; Krayevska, Y.A.; Yaschuk, V.P. Synthesis and crystal structure of BaLn<sub>2</sub>In<sub>2</sub>O<sub>7</sub>. *Rep. Natl. Acad. Sci. Ukr.* **2010**, *1*, 148–153.
47. Caldes, M.; Michel, C.; Rouillon, T.; Hervieu, M.; Raveau, B. Novel indates Ln<sub>2</sub>BaIn<sub>2</sub>O<sub>7</sub>, n = 2 members of the Ruddlesden–Popper family (Ln = La, Nd). *J. Mater. Chem.* **2002**, *12*, 473–476. [[CrossRef](#)]
48. Momma, K.; Izumi, F. VESTA 3 for three-dimensional visualization of crystal, volumetric and morphology data. *J. Appl. Crystallogr.* **2011**, *44*, 1272–1276. [[CrossRef](#)]